



Published in final edited form as:

Nat Geosci. 2019 May ; 12(May): 333–338. doi:10.1038/s41561-019-0345-3.

Lunar soil hydration constrained by exospheric water liberated by meteoroid impacts

M. Benna^{1,2,*}, D. M. Hurley³, T. J. Stubbs¹, P. R. Mahaffy¹, R. C. Elphic⁴

¹NASA Goddard Space Flight Center, Greenbelt, MD, USA.

²CSST, University of Maryland, Baltimore County, Baltimore, MD, USA.

³The Johns Hopkins University Applied Physics Laboratory, Laurel, MD, USA.

⁴NASA Ames Research Center, Moffett Field, CA, USA.

Abstract

Analyses of samples from the Apollo missions suggest that the Moon formed devoid of native water. However, recent observations by Cassini, Deep Impact, Lunar Prospector and Chandrayaan-1 indicate the existence of an active water cycle on the Moon. Here we report observations of this water cycle, specifically detections of near-surface water released into the lunar exosphere by the Neutral Mass Spectrometer on the Lunar Atmosphere and Dust Environment Explorer. The timing of 29 water releases is associated with the Moon encountering known meteoroid streams. The intensities of these releases reflect the convoluted effects of the flux, velocity and impact location of the parent streams. We propose that four additional detected water releases represent the signature of previously undiscovered meteoroid streams. We show that water release from meteoroid impacts is indicative of a lunar surface that has a desiccated soil layer of several centimetres on top of uniformly hydrated soil. We infer that the Moon is currently in the process of losing water that was either delivered long ago or present at its formation.

*Correspondence and requests for materials should be addressed to M.B. mehdi.benna@nasa.gov.

Author contributions

M.B. directed the data analysis and was primarily responsible for writing the article. D.M.H. developed the exosphere model and helped analyse and interpret the NMS data. T.J.S. conducted the correlation analysis between meteoroid streams and the NMS observations. P.R.M. is the principal investigator of the instrument and contributed to instrument calibration and data analysis. R.C.E. is the LADEE project scientist, developed the LADEE observation plans for the NMS, coordinated data acquisition with other LADEE instruments and contributed to data analysis.

Competing interests

The authors declare no competing interests.

Additional information

Supplementary information is available for this paper at <https://doi.org/10.1038/s41561-019-0345-3>.

Reprints and permissions information is available at www.nature.com/reprints.

Publisher's note: Springer Nature remains neutral with regard to jurisdictional claims in published maps and institutional affiliations.

Data availability

The NMS data supporting this Article are publicly available from the Planetary Data System (http://pds-atmospheres.nmsu.edu/data_and_services/atmospheres_data/LADEE/nms.html).

Code availability

The Matlab scripts used for the analyses and modelling described in this study can be obtained from the corresponding author on reasonable request.

The quest to find signs of water on the surface of the Moon has been the subject of extensive research and intense debates. Following the early analysis of lunar samples from the Apollo and Luna missions, the surface was generally accepted to be anhydrous^{1–4}. Recently, this consensus was challenged due to spectroscopic observations by Cassini, Deep Impact and Chandrayaan-1 that provided evidence of a global lunar surface hydration of ~10–1,000 ppm of H₂O/OH (refs. ^{5–7}). In addition, an enhanced concentration of hydrogen attributed to the presence of larger water ice deposits in the permanently shadowed craters of the poles was detected by the Lunar Prospector Neutron Spectrometer (LPNS)⁸. This observation was subsequently confirmed by the neutron detector onboard the Lunar Reconnaissance Orbiter⁹ and the impact experiment of the Lunar Crater Observation and Sensing Satellite¹⁰. These ice deposits are believed to originate from water released by impacts on the lunar surface^{11,12}. Hydrated meteoroids (such as type-I carbonaceous chondrites) and comets can release their water content into the exosphere following lunar impact and simultaneously liberate water synthesized from the reduction of soil FeO by solar wind-implanted hydrogen in agglutinates¹³. A portion of the water released may migrate to cold traps in the permanently shadowed regions (PSRs), where it may remain thermally stable for billions of years^{12,14}.

Elements of this lunar water cycle have been modelled (including water synthesis by solar wind implantation, water release by meteoroids and subsequent lateral transport of water across the exosphere^{15–17}), but not yet observed and characterized. Key questions remain as to whether the bulk of the impact-released water is sourced from the surface, and whether meteoroid impacts can sustain a measurable water exosphere around the Moon. It is also unclear whether the impact process is efficient enough to be a viable source of the water trapped in the PSRs at the poles, and how water concentration varies with depth in the lunar regolith. The LPNS measured a bulk concentration of 180–1,350 ppm of water-equivalent hydrogen in the top metre of soil of the equatorial high-lands (with a global average of 585 ppm), presumed to be of solar origin¹⁸. However, global mapping of the same regions using the spectral data of Chandrayaan-1 did not yield measurable water in the top millimetre of the soil¹⁹. Here we report observations from the Neutral Mass Spectrometer (NMS) onboard the Lunar Atmosphere and Dust Environment Explorer (LADEE) that address these outstanding questions.

NMS observations of exospheric water

During its eight-month mission, the LADEE spacecraft collected measurements of the composition of the lunar exosphere²⁰ using the NMS instrument²¹, powered on regularly for tens of minutes of measurement activity. Key volatiles, including He, Ne, Ar and CH₄ (refs. ^{22,23}), were mapped and other species were detected as pickup ions²⁴. Analysis of the water sampled during periods of inactivity (Supplementary Materials 1–3) reveals that fluctuations in the mass-per-charge 18 water channel reflect the abundance of water molecules in sorption equilibrium between the gas phase and the internal surfaces of the sensor. This provides a measure of the quantity of water-group molecules ingested by the instrument during the most recent period of inactivity. The fluctuations thus capture variations in the underlying source of the water released into the exosphere. The data reduction procedure that allows us to quantify the flux of water into the NMS is described in the Methods and

Supplementary Material 1. The NMS instrument cannot resolve whether the parent exospheric molecule of the measured water is H₂O or OH due to surface reactions between OH and H, and so we will refer to water-group molecules (H₂O and OH) as water.

Over the course of the LADEE mission science phase (November 2013–April 2014), the NMS collected 743 independent measurements of water abundances shortly after the instrument was switched/turned on. These measurements reflect the abundance of exospheric water that was ingested by the sensor at typical altitudes of 20–100 km along the near-equatorial orbit of LADEE, which ranged $\pm 23^\circ$ in latitude, and over typical periods of instrument inactivity lasting 10–1,300 min (median duration of 129 min). All water abundance measurements are depicted in Supplementary Fig. 1. The median density is 22.8 cm⁻³, with a median absolute deviation (MAD) of 11.8 cm⁻³. Of these measurements, 736 have an abundance level above 3σ of their random uncertainties and are considered to represent positive detection of exospheric water. These measurements are referred to as water events in this study. The lowest-intensity water event is recorded at 5.7 cm⁻³, which sets a new upper limit of 0.62 cm⁻³ for steady-state density in any potential permanent water exosphere. Furthermore, a total of 214 episodic and short-lived intense events (with intensities >10 times the median intensity of the entire collection of events) were recorded. These high-intensity events were concentrated in the period from mid-November 2013 to mid-January 2014, during which the Moon encountered a series of well-known and annually occurring strong meteoroid streams (for example, the Leonids, Geminids and Quadrantids). The frequency and magnitude of these high-intensity events steadily declined in the early months of 2014 before increasing again in early April 2014. There is no discernible correlation between the duration of the period of inactivity and the intensity of the subsequent water measurement (Supplementary Fig. 2), demonstrating that the observed measurement is due to variations in water density in the exosphere on scales of minutes to a few hours, rather than differences in the duration of the periods of inactivity. The water events recorded by the NMS capture the signatures of meteoroid strikes on the lunar surface due to three impactor populations: meteoroid streams, sporadic background meteoroid flux and large isolated meteoroids. Due to their predictable nature, we used meteoroid streams to demonstrate the unequivocal correlation between impacts and recorded water signatures.

Correlation with known meteoroid streams

According to the International Astronomical Union (IAU) Meteor Data Center (MDC) list of established meteor showers observed at Earth²⁵, 40 annual meteoroid streams organized in 32 temporally distinct stream groups should have encountered the Moon during the LADEE science phase (see Methods). These streams are relatively well characterized and broad enough to reasonably assume that both the Earth and Moon would have passed through them. During the encounter between the Moon and the strongest streams, the Lunar Dust Experiment (LDEX) observed an increase in the density of ejected dust particles, providing a clear stream signature²⁶. To correlate the events observed by the NMS with known meteoroid streams, a metric of normalized event intensity rate (NEIR) was calculated (Supplementary Material 6). Events that occur with high intensity and high cadence register as high values on this metric and are observed as distinct extrema. However, this metric returns low values if the events occur at lower intensity and/or lower cadence. Figure 1

presents the calculated NEIR with its relevant uncertainties. From this profile, an automatic algorithm isolated 44 atypical extrema organized in 39 peak events. A degree of statistical significance quantifies how atypical these outlier events are compared to the bulk of the NMS-recorded water events.

Supplementary Table 1 shows that most of the peak events coincided in time with established meteoroid streams (see Methods). Twenty-nine of these peaks occurred within 48 h of the expected maximum flux for a stream group (15 peaks occurred within 12 h, 12 peaks within 24 h, and 2 peaks within 48 h). Strong meteoroid streams with near-equatorial radiants (such as the Leonids and Geminids) produce several large events at high cadence, whereas smaller showers (such as the Ursids and α -Centaurids) yield lower-intensity events at modest rates. Fourteen of these peak events have a degree of statistical significance $>16 \times$ MAD, making them unequivocal departures from stochastic randomness. Although 29 of 32 established stream groups are accounted for in the NMS-observed peak events, 1 did not yield a noticeable signature, and a further 2 occurred during a period when the instrument was not operating. In comparison, LDEX detected dust signatures for only three established streams in the same period²⁶. The lack of a noticeable permanent water exosphere made meteoroid stream signatures more prominent and discernable by the NMS (see Methods). In contrast, the LDEX dust measurements are dominated by the pronounced signature of the background dust cloud of the Moon, from which only a few streams were intense enough to emerge²⁷. The effectiveness of the NMS at detecting meteoroid streams was further enhanced by the fact that impact-generated water molecules have large and global ballistic trajectories¹⁶, which gives the NMS a Moon-wide view of the exosphere. While the sensitivity of the NMS to a given meteoroid stream is biased towards radiants at equatorial latitudes, it remains relatively high even at the most extreme angles (see Methods and Supplementary Fig. 3).

Figure 1 depicts ten peak events that could not be attributed to any established streams. Six are of low intensity and/or a low degree of significance and can be reasonably attributed to a few of the weaker showers reported on the MDC's working list. However, four unidentified peak events (events 15, 34, 35 and 37, which occurred at 09:36 UT on 9 January 2014, 4:48 UT on 2 April 2014, 14:24 UT on 5 April 2014 and 7:12 UT on 9 April 2014, respectively) represent the discovery of new streams. These peaks are too strong, have a high degree of significance and are too well defined to be explained by any of the weaker streams on the MDC's working list.

To further confirm the causal link between meteoroid streams and the NMS-observed water events, we compared the magnitudes of the peak events that were identified as being the Geminids, Ursids and Quadrantids with contemporaneous observations reported by the International Meteor Organization (IMO) network²⁸ (see Methods). As expected, the intensities of the three peak events observed by the NMS reflect the convoluted effect of the flux, velocity and impact location of their parent streams. In addition, a comparison between the NMS- and IMO-observed temporal profiles of the Geminid shower confirms that the NMS data captures the correct evolution and width of the stream (see Methods).

These analyses provide unambiguous evidence that the NMS captures the fluctuations in the abundance of water released into the exosphere following meteoroid impacts. These fluctuations provide information on the nature of the meteoroids that triggered the water release into the exosphere, and the nature of the reservoir that sequestered the water beforehand.

Implications for lunar soil hydration

A comparison of the NMS measurements with LDEX observations and an exosphere model (see Methods and Supplementary Materials 4 and 5) shows that the mass flux of released water is largely generated by meteoroids in the 0.15 g – 1×10^6 g mass range, with smaller meteoroids providing minimal contributions to the water exosphere (see Methods). This can only be the case if the top few centimetres of the lunar regolith are desiccated. By allowing for the presence of a desiccated top layer in the model, and accounting for the volume of the soil that is shocked above the desorption threshold, we were able to fit the distribution of the data (Fig. 2). The best match is achieved with a desiccated layer thickness of $8.0 \text{ cm} \pm 1.0 \text{ cm}$. Only meteoroids with a mass larger than 0.15 g are able to pierce this dry stratum and excavate deeper soils. An average of 220–520 ppm by weight of H_2O is required below this desiccated layer to reflect the intensity of the observed events. This water concentration is constant to a depth of at least 3 m, which reflects the maximum penetration of impacting meteoroids of 100 kg (99% of the amplitude of the observed data is generated by meteoroids in the 0.15 g–100 kg range). In the fitting process, the cutoff impactor mass that is effective at releasing water is the only parameter that dictates the relative profile (that is, the shape) of the resulting distribution of the measurements. The relatively low random errors ($\pm 15\%$ at 1σ) in the data provide a high level of confidence in the derivation of these characteristics. The concentration in the soil underlying the desiccated layer affects only the linear scaling of the intensity of the observed events. As such, the derived hydration level bears the same systematic error of $\pm 30\%$ (1σ) as the NMS measurements. As the sensitivity of the NMS to water releases is biased towards low latitudes, the derived thickness is an average applicable to the equatorial regions.

Although the presence of a desiccated top layer was expected based on the spectral observations of the lunar equatorial region¹⁹, the NMS measurements show that its thickness extends beyond the top millimetre of the soil. The reported thickness is commensurate with the depth at which diurnal equatorial temperatures range between 220–255 K, compared to 100–380 K at the surface²⁹. This indicates that water has a short lifetime within the thermally active surface layer because it is rapidly transported by thermal desorption and diffusion upwards to the surface, or downwards deeper into the soil. It can be lost from the surface by sputtering, photon-stimulated desorption and thermal desorption (Fig. 3). Thermal control of the desiccated layer implies its potential thinning at higher latitudes with shallower isotherms³⁰. Deeper in the soil, water can be sequestered³¹. Although the desiccated layer acts as a bridge between the surface, where most of the water is formed (most probably from reduction of soil FeO by solar wind-implanted hydrogen in agglutinates), and deeper soil, where the water can be stored, it harbours within itself a very low concentration of water (Fig. 3). The NMS observations suggest that the water

concentration below the desiccated layer remains uniform, indicating that the adsorbed water permeates the regolith.

As described in the Methods, our analysis reveals that nearly all of the water is sourced from adsorbed water below the desiccated layer, and not from vapour and melts produced during impact from the meteoroid itself.

Global water cycle budget on the Moon

The impact release of water vapour from the lunar regolith contributes to the overall loss of water from the Moon. The data show that $1.3 \times 10^{-17} - 3.2 \times 10^{-17} \text{ g cm}^{-2} \text{ s}^{-1}$ of water is released globally by meteoroid impacts. This amounts to a total of $5.1\text{--}12.1 \text{ g s}^{-1}$ that can potentially be lost to space, assuming that the surface properties inferred from the equatorially biased NMS observations are applicable at higher latitude. This loss rate would be higher if the desiccated layer was thermally controlled, such that its thickness decreased at higher latitude. Our exosphere model shows that impact vapour plumes are energetic and that an average of 67% of the vapour exceeds the escape velocity from the Moon and is lost. The remaining 33% is redeposited on the surface after lateral transport in the exosphere. Therefore, the water loss rate due to meteoroid impact is $3.4\text{--}8.1 \text{ g s}^{-1}$. The average solar water production rate was estimated at 2.0 g s^{-1} on the basis of the ratio of the abundance of metallic iron in the regolith to the age of the regolith^{12,32}. In the absence of any other major endogenic reservoir, the net water loss rate at the Moon that results from the balance between solar wind synthesis and loss by meteoroid impact is $1.4\text{--}6.1 \text{ g s}^{-1}$. Other minor loss processes, such as solar wind sputtering, will contribute to the loss but may be negligible if a desiccated top layer is present. The resulting surface loss/gain ratio is $\sim 1.6\text{--}4:1$. This ratio does not apply locally to the PSRs, in which the dominant source of replenishment comes mainly from the redeposition of water that was excavated elsewhere by impacts. With their higher water concentration compared to the lunar average, the PSRs suffer a much higher net loss from meteoroid impacts. If we assume ice-deposit concentrations of 0.5% by weight⁸, the water loss by impacts in the 0.08% surface fraction of the PSRs³³ is equal to 5,000:520–220 ppm, which is between 9.6–22.7 times the derived global water release rate. This amounts to a total of $9.3 \times 10^{-2} \text{ g s}^{-1}$. In comparison, we calculate the average rate of replenishment by migration and deposition of water that was excavated elsewhere on the same surface area to be a negligible at $1.3 \times 10^{-3} - 3.2 \times 10^{-3} \text{ g s}^{-1}$. Therefore, the water deposits at the PSRs undergo a faster rate of erosion with a loss/gain ratio of $\sim 30\text{--}70:1$. In conclusion, the Moon—and particularly the PSRs—most probably has a net water loss regime. To sustain this loss rate over geological time, the water must have been delivered long ago, or it was present at lunar formation.

Figure 3 synthesizes our proposed view of the stratification of the lunar surface and the pathways through which water is formed, exchanged, transported and ultimately lost. This figure emphasizes the reservoirs and pathways that were characterized through analysis of the NMS observations. While this figure is not comprehensive, it puts our results in the context of what was already established or hypothesized.

Online content

Any methods, additional references, Nature Research reporting summaries, source data, statements of data availability and associated accession codes are available at <https://doi.org/10.1038/s41561-019-0345-3>.

Methods

Overview of NMS measurements and the data reduction method.

The NMS is a quadrupole mass analyser that utilizes a dual-ion source designed to measure both surface-reactive and inert species in the mass range $m = 2\text{--}150$ Da with a unit mass resolution ($m = 1$ Da). During the science phase of the mission, the instrument was turned on regularly for a typical duration of 30–60 min to measure the composition of the exosphere. Operations were interleaved with periods of inactivity, during which the instrument surfaces were cold and remained exposed to the exospheric environment. The NMS instrument targeted water-group molecules and other species as part of its nominal observation sequence.

The data reduction procedure focused on isolating and extracting a subset of data for thermalized neutral gas measured in closed-source mode at mass-to-charge ratio $m/z = 18$. The measurements of interest were recorded during the first 5 min following turn-ons of the NMS. After the first few minutes, outgassing from the filament and walls of the rapidly warming sensor irrevocably destroyed the state of sorption equilibrium that was established when the surfaces of the instrument were cold. After the completion of its scheduled operation, the instrument was turned off, and the freshly baked internal walls of the sensor rapidly cooled down and resumed adsorbing any exospheric water encountered during the subsequent period of inactivity. The data extracted from the early moments of the activities of the instrument were subsequently corrected for background trends and temperature effects, and were reduced to a set of abundance measurements (Supplementary Fig. 1). Each measurement $n_{s,i}(t_{\text{on},i})$ of water abundance n_s in the source collected at the start time $t_{\text{on},i}$ of activity i is proportional to the contribution of the integrated density of exospheric water n_e that was ingested during the instrument period of inactivity t_p and of exospheric water subjected to the instrument at the time of the measurement:

$$n_{s,y}(t_{\text{on},t}) \propto An_e(t_{\text{on},t}) + (A - 1) \int_{\Delta t} n_e(t)r_s(t)dt \quad (1)$$

The function $r_s(t)$ is an intrinsic property of the instrument that captures its retention of water, or ‘memory’. The constant A sets the balance between the contributions of the present and memorized states of the exosphere. Further details on the derivation of equation (1) are provided in Supplementary Materials 2.

Correlation of the NMS observations with known meteoroid streams.

The IAU’s online MDC database archives information on hundreds of reported meteor showers from multiple sources²⁵. The primary objective of the MDC is to maintain a

descriptive list of the established meteor showers that have been recognized with an official name and number by the IAU. This database is continuously evolving as more observations are collected and verified, so it is important to acknowledge that the MDC list of meteor showers used was updated on 18 January 2018, and contained 112 established meteor showers and 565 working meteor showers²⁸. Working showers are those that have been reported but have not fulfilled the IAU verification criteria for established showers. In our study, we compare the water events observed by the NMS with the occurrence of meteoroid streams that produce the established meteor showers. The MDC database often provides parameters for individual showers from more than one set of independent measurements. One of the parameters included is the zenithal hourly rate (ZHR), which corresponds to the number of meteors an observer would see in an hour of peak activity under optimal viewing conditions.

Temporal correlation.

The MDC database provides the solar longitude of the Earth (J2000) during the observed peak in meteor shower activity. Solar longitude provides the precise position of the Earth in its orbit as an angular distance from the intersection of the ecliptic and celestial equators. The solar longitude during peak shower activity typically remains consistent year to year, whereas the vagaries of the calendar mean that the date and time can vary by several hours on consecutive years. As we are making a comparison with observations from lunar orbit, we also corrected for the small, but sometimes significant, offset between the solar longitude of the Earth and the Moon; for example, if the Moon is ahead of the Earth in its orbit around the Sun, we would expect it to encounter the meteoroid stream earlier. We made this adjustment using the position of the Moon relative to the orbital direction of the Earth (the y axis of the Geocentric Solar Ecliptic coordinate system), and also accounted for the different radii of the Earth and Moon. We converted solar longitude to universal time using the formula for the J2000 epoch³⁷.

Supplementary Table 1 provides the list of meteoroid streams predicted to encounter the Moon during the science phase of the LADEE mission, and includes the estimated times of peak activity, as well as the typical peak ZHR when available. However, when predicted peak times for the same meteoroid stream were separated by more than a day, we treated them as separate streams when comparing to NMS observations. When several streams were coincident in time, they were grouped and treated as a single stream (referred to as a stream group). The predicted timing of streams in Supplementary Table 1 are compared with the timing of the peak events identified in Supplementary Materials 6. Peak events that fall within 48 h of an established stream are considered a match. Peak events with timings that do not correspond to that of any established streams, but may correspond to one of the weaker streams from the MDC working meteor list, are flagged as possible matches. Strong peak events with timings that do not correspond to that of any established stream but cannot possibly correspond to one of the weaker streams from the MDC working meteor list are flagged as new streams.

Validity of the intensities of the observed peak events.

During an encounter between the Moon and a given meteoroid stream, the intensity of the NMSobserved signature is expected to convolve the effects of:

- Stream peak flux
- Stream impact velocity
- Stream particle size distribution and composition
- Elevation angle of stream radiant with respect to the orbital plane of LADEE at the time of peak activity
- Dependency of NMS sensitivity on impact location

Of all the established streams that were expected to encounter the Moon during the course of the LADEE mission, only the Geminids, Ursids and Quadrantids were characterized and reported by the IMO²⁸. The ZHRs recorded at the peak of each stream's activity in 2013–2014 were compared to the observed magnitude of the corresponding peak event in the NMS data (peaks 6, 8 and 13 in Fig. 1). In the absence of information about the relevant particle size distribution and composition for each stream, we assumed that the Geminids, Ursids and Quadrantids share similar impactor properties. Supplementary Table 2 captures information on peak flux, impact velocity and radiant elevation for these three streams. These parameters were used in the water exosphere model (described in Supplementary Materials 4) to generate the synthetic NMS observations that would result from a collimated stream with a normalized impact flux and a given radiant elevation.

Supplementary Fig. 3 shows the median magnitude of the expected NMSobserved events that would result from Geminid-, Ursid- and Quadrantid-like streams. It also provides the dispersion of these intensity values (25th–75th percentile range) that is due to the stochastic variability of observation start times and durations. The magnitudes shown in Supplementary Fig. 3 were scaled by the IMO-reported intensity of each stream to provide a common base of comparison. This figure reveals that while the Quadrantid stream had a peak flux comparable to that of the Geminids (ZHR $\sim 120 \text{ hr}^{-1}$), its higher radiant elevation and faster impact speed were expected to generate an NEIR magnitude that is $3.5\times$ weaker. The NMS observations are within 15% from this expected value. In contrast, the analysis shows that, owing to their slower impact speed, the Ursids were expected to yield an NMS signature with $1.5\times$ the magnitude of that of the Geminids for an equal radiant elevation and equivalent stream flux. This magnitude is reduced by 68% when the higher elevation of the radiant of the Ursids is accounted for. The NMS observations are within 28% of this expected value. In addition, Supplementary Fig. 3 shows that the deviations between the expected and observed peak event magnitudes are within the uncertainties of the NMS and IMO observations.

It should be noted that the water yield of the meteoroid streams decreases as impact speed increases. This stems from the fact that the shockwave that expands across the impact site decays more rapidly for faster impact speeds (reflected by Supplementary Fig. 14 and equation (35) in the Supplementary Materials) due to energy loss in heating, melting and vapourizing of material behind the shockfront³⁸. This faster shockwave attenuation results in

a smaller volume of soil within the threshold energy of water desorption, and ultimately in lower water production.

Validity of the observed event profile for the Geminids.

The full-width at half-maximum (FWHM) of the peak events identified in the NEIR time series ranges from 0.7 to 2.1 days for the narrowest and widest peak events, respectively. The FWHM is expected to reflect the time span during which each meteoroid stream was active enough to release an atypical amount of water into the lunar exosphere. One should be aware that the moving average applied to the NMS data during processing (Supplementary Material 6) widens the apparent FWHM of the observed streams by up to 0.5 days. Of all the streams that were concurrent to the NMS operation period, the Geminid shower was the only stream extensively monitored by the IMO Video Monitor Network³⁹. Note that historical data that were reported for other showers⁴⁰ lack the temporal resolution and precision to render the exact structures of streams during the peak of their activities with a quality that can be reasonably compared with the NMS observations.

Supplementary Fig. 4 presents a comparison between the IMO-reported flux density profile of the Geminids and the NMS-observed evolution of the NEIR during the same ± 3 -day period. To account for the effect of the averaging that was applied to the NMS data, the IMO observations were subjected to analogous Gaussian-weighted averaging, with a FWHM of 0.5 days. As expected, this averaging process artificially widened the FWHM of the IMO-observed flux density from 1.25 to 1.6 days. This larger FWHM is comparable to that of the NMS-observed profile. The figure also shows that despite the coarser measurement cadence of the NMS observations, its temporal evolution closely tracks that of the IMO observations. This provides further evidence that the temporal evolutions of the observed NMS peak events track those of their temporally coincident established streams.

Evidence for a desiccated surface layer.

The observed events provide information on the efficiency of water extraction from the lunar soil by meteoroids with masses that range from 10^{-12} – 10^6 g. Impactors larger than 10^6 g have an impact rate of 1 every 17 years³⁶ and are less likely to have occurred during the course of the LADEE mission (less than 4% probability). Impactors smaller than 10^{-12} g amount to less than 0.5% of the total mass flux striking the Moon³⁴ and are expected to have a negligible contribution to any induced water exosphere. For a given impactor speed and density, as the depth of the excavated target material scales linearly with the impactor diameter⁴¹, the observed water events can provide information about the average variation with depth of water concentration in the lunar subsurface in a statistical sense. In this study, information about soil hydration was extracted by comparing the distribution of the intensity of the observed water events against the distribution that would result from a given impactor flux distribution. Details of the exosphere and impactor flux models are provided in Supplementary Material 4.

The comparison between the data and the model (Fig. 2) shows that if water released from the lunar surface by the entirety of the meteoroid complex mass range (10^{-12} – 10^6 g) is considered, a permanent water exosphere would form. This water exosphere would have

relatively small temporal variability and lack large fluctuations, such as those observed by the NMS. In this ‘featureless’ permanent water exosphere, the variation coefficient of the distribution of synthetic observations would be 0.11, whereas it is 1.34 in the NMS data. As a consequence, the distribution of the intensity of synthetic observations of water events (Fig. 2b) would mimic the distribution of the duration of period of inactivity (Supplementary Fig. 10), which is very different from that of the actual NMS observations. As shown in Supplementary Fig. 2, the NMS observations do not correlate with the duration of the inactivity period of the instrument. The featureless nature of the synthetic exosphere is due to the fact that the impactor mass flux, and thus the mass flux of released water, is produced largely by meteoroids in the 10^{-8} – 10^{-2} g mass range (Fig. 2a). These micrometeoroids generate a sustained water exosphere to which meteoroids larger than 1 g contribute with a water flux of less than 4%. The NMS does not reveal the presence of any permanent water exosphere (above 0.62 cm^{-3}), and the NMS data show that the detected episodic water events have signatures much more pronounced than would be generated by the full meteoroid complex. The inconsistency between the data and model that involves the entire meteoroid complex strongly suggests that, unlike large meteoroids, impacts of micrometeoroids ($< 0.15 \text{ g}$) are very inefficient at releasing water into the exosphere. This would be the case if the top few centimetres of the lunar regolith are desiccated.

The same conclusion can also be derived from a comparison of NMS observations with those of LDEX. The NMS NEIR (Fig. 1) is analogous in its meaning to the one-day averaged dust impact rate of LDEX. The LDEX instrument detected a permanent dust cloud on the Moon that formed following meteoroid bombardment²⁶. The magnitude of variations in the permanent dust cloud are captured in the coefficient of variation of dust impact rates on the detector. This ratio is equal to 0.19 for dust size $>0.3 \mu\text{m}$. Both water molecules and dust ejecta are the by-products of meteoroid impacts and thus they respond similarly to variations in fluxes and physical properties of the impactors (the mass of solid ejecta and vapours scale similarly to functions of impactor mass and speed⁴¹). If the Moon did not have a desiccated layer, and water was continuously released by impacts regardless of impactor size and speed (similarly to the dust ejecta), the NMS would have detected a permanent water exosphere. This water exosphere would vary statistically, with trends and amplitudes similar to those of the permanent dust cloud. The NMS would have captured this variation in the derived intensity event rates with a coefficient of variation equal to 0.19. The NMS instead measured a coefficient value of 0.92, representing variations that are ~ 5 times larger than those observed in the permanent dust cloud by the LDEX. A variation coefficient equal to 0.19 would have generated a mean intensity event rate of 203 instead of the observed value of 41 (Fig. 1). The inconsistencies between the behaviours of NMS-observed water events and LDEX-detected dust is consistent with the presence of a dry top layer covering hydrated soils. This desiccated layer allows the more frequent micrometeoroids to generate and sustain a permanent dust cloud, while precluding them from accessing the water reserves underneath and, consequently, from producing a permanent water exosphere. When this desiccated layer is breached by the larger and faster impactors of meteoroid streams (the mass distribution of streams are typically biased towards more massive particles with speeds $>30 \text{ km s}^{-1}$ (ref. ⁴⁰))—although the sporadic background is biased towards smaller particles

with speeds $<15 \text{ km s}^{-1}$)—the released water expands broadly around the Moon and is detected by the NMS as episodic, but very pronounced, water events.

Source of the released water.

To account for the relatively large intensities of the detected events, our analysis reveals that impacts must yield an amount of water 5.4–12.8 times the impactor mass (Supplementary Material 5). The impactor itself cannot be the prevailing source of the observed water as its water content is only a few tenths to a few per cent of its overall mass⁴². The vapour and the melts that are produced during an impact can also be discounted as the main source of the water. Typically, the melted and vapourized mass in the target material is <200 times the impactor mass⁴³, and their content in devolatilized water would be equal to one impactor mass at most. The released water cannot therefore originate from structural water in hydrous minerals, which requires high shock pressures to devolatilize to melts and vapours⁴⁴. Instead, it most probably comes from adsorbed water on regolith grains that is desorbed by the shockwave that expands across the impact site. The activation energies of desorption of physisorbed and chemisorbed water on lunar regolith samples and analogues were measured to be 144–158 kJ mol^{-1} (refs. ^{45,46}). This threshold energy can be delivered by shock pressures as low as 100 MPa. In a typical impact of a meteoroid on the porous lunar soil, the excavated material within the volume of the crater is subjected to peak shock pressures in excess of 500 GPa (ref. ³⁸), and shockwave pressures will remain above the threshold required for water desorption to distances of several crater radii. The fact that the water concentration that we derived for the deeper soil is commensurate to the average 585 ppm measured in the first top metre by the LPNS¹⁸ supports the assumption that shock-induced outgassing acts beyond the confines of the volume of the excavated crater and extends to the surrounding soils.

Supplementary Material

Refer to Web version on PubMed Central for supplementary material.

Acknowledgements

The LADEE/NMS investigation was supported by NASA. Tests and calibrations were completed at the Planetary Environment Laboratory of NASA's Goddard Space Flight Center. We thank R. R. Vondrak, W. M. Farrell, R. M. Killen and T. H. Morgan for insightful discussions and comments. We also thank E. Raaen for his calibration support, E. Zubritsky for editing and J. Friedlander for graphics assistance.

References

1. Taylor SR Lunar Science: A Post-Apollo View (Pergamon, 1975).
2. Papike JJ, Taylor L. & Simon S. in The Lunar Source Book (eds Heiken GH. et al.) 121–182 (Cambridge Univ. Press, 1991).
3. Lucey P. et al. Understanding the lunar surface and space–Moon interactions. *Rev. Miner. Geochem* 60, 83–219 (2006).
4. Shearer CK et al. Thermal and magmatic evolution of the Moon. *Rev. Miner. Geochem* 60, 365–518 (2006).
5. Clark RN Detection of adsorbed water and hydroxyl on the Moon. *Science* 326, 562–564 (2009). [PubMed: 19779152]

6. Sunshine JM et al. Temporal and spatial variability of lunar hydration as observed by the Deep Impact spacecraft. *Science* 326, 565–568 (2009). [PubMed: 19779149]
7. Pieters CM et al. Character and spatial distribution of OH/H₂O on the surface of the Moon seen by M³ on Chandrayaan-1. *Science* 326, 568–572 (2009). [PubMed: 19779151]
8. Feldman WC et al. Fluxes of fast and epithermal neutrons from lunar prospector: evidence for water ice at the lunar poles. *Science* 218, 1496–1500 (1998).
9. Mitrofanov IG et al. Mapping of the lunar south pole using the LRO neutron detector experiment LEND. *Science* 330, 483–486 (2010). [PubMed: 20966247]
10. Colaprete A. et al. Detection of water in the LCROSS ejecta plume. *Science* 330, 463–468 (2010). [PubMed: 20966242]
11. Watson K, Murray B. & Brown H. On the possible presence of ice on the Moon. *J. Geophys. Res* 66, 1598–1600 (1961).
12. Arnold JR Ice in the lunar polar regions. *J. Geophys. Res* 84, 5659–5668 (1979).
13. Housley RM, Cirlin EH & Grant RW Characterization of fines from the Apollo 16 site. *Geochim. Cosmochim. Acta* 3, 2623–2642 (1974).
14. Urey HC *The Planets, Their Origin and Development* (Yale Univ. Press, 1952).
15. Crider DH & Vondrak RR Space weathering effects on lunar cold trap deposits. *J. Geophys. Res* 108, 5078 (2003).
16. Hurley DH & Benna M. Simulations of lunar exospheric water events from meteoroid impacts. *Planet. Space Sci* 162, 148–156 (2017).
17. Prem P, Artemieva NA, Goldstein DB, Varghese PL & Trafton M. Transport of water in a transient impact-generated lunar atmosphere. *Icarus* 255, 148–158 (2015).
18. Lawrence DJ et al. Bulk hydrogen abundances in the lunar highlands: measurements from orbital neutron data. *Icarus* 255, 127–135 (2015).
19. Li S. & Milliken RE Water on the surface of the Moon as seen by the Moon Mineralogy Mapper: distribution, abundance, and origins. *Sci. Adv* 3, e1701471 (2017).
20. Elphic RC et al. The Lunar Atmosphere and Dust Environment Explorer mission. *Space Sci. Rev* 185, 3–25 (2014).
21. Mahaffy PM et al. The Neutral Mass Spectrometer on the Lunar Atmosphere and Dust Environment Explorer mission. *Space Sci. Rev* 185, 27–61 (2014).
22. Benna M, Mahaffy PR, Halekas JS, Elphic RC & Delory GT Variability of helium, neon, and argon in the lunar exosphere as observed by the LADEE. *Geophys. Res. Lett* 42, 3723–3729 (2015).
23. Hodges RR Jr Methane in the lunar exosphere: implications for solar wind carbon escape. *Geophys. Res. Lett* 43, 6742–6748 (2016).
24. Halekas JS et al. Detections of lunar exospheric ions by the LADEE neutral mass spectrometer. *Geophys. Res. Lett* 42, 5162–5169 (2015).
25. Jopeka TJ & Ka uchová Z. IAU Meteor Data Center—the shower database: a status report. *Planet. Space Sci* 143, 3–6 (2017).
26. Horányi M. et al. A permanent, asymmetric dust cloud around the Moon. *Nature* 522, 324–326 (2015). [PubMed: 26085272]
27. Szalay JR & Horányi M. Detecting meteoroid streams with an in-situ dust detector above an airless body. *Icarus* 275, 221–231 (2016).
28. International Meteor Organization (accessed 18 January 2018); <http://www.imo.net/>
29. Vasavada AR et al. Lunar equatorial surface temperatures and regolith properties from the Diviner Lunar Radiometer Experiment. *J. Geophys. Res* 117, E00H18 (2012).
30. Hayne PO et al. Global regolith thermophysical properties of the Moon from the Diviner Lunar Radiometer Experiment. *J. Geophys. Res* 122, 2371–2400 (2017).
31. Schorghofer N. & Aharonson O. The lunar thermal ice pump. *Astrophys. J* 788, 169 (2014).
32. Housley RM, Grant RW & Paton NE Origin and characteristics of excess Fe metal in lunar glass welded aggregates. *Geochim. Cosmochim. Acta* 3, 2737–2749 (1973).
33. Mazarico E. et al. Illumination conditions of the lunar polar regions using LOLA topography. *Icarus* 211, 1066–1081 (2011).

34. Grün E, Zook HA, Fetchtig H. & Giese RH Collisional balance of the meteoritic complex. *Icarus* 62, 244–272 (1985).
35. Halliday I, Griffin AA & Blackwell AT Detailed data for 259 fireballs from the Canadian camera network and inferences concerning the influx of large meteoroids. *Meteorit. Planet. Sci* 31, 185–217 (1996).
36. Brown P, Spalding RE, ReVelle DO, Tagliaferri E. & Wordenk SP The flux of small near-earth objects colliding with the Earth. *Nature* 420, 294–296 (2002). [PubMed: 12447433]
37. Steyaert C. Calculating the solar longitude 2000.0. *WGN* 19, 31–34 (1991).
38. Melosh HJ *Impact Cratering: A Geologic Process* 60–65 (Oxford Univ. Press, 1989).
39. Molau S. et al. Results of the IMO Video Meteor Network—December 2015. *WGN* 44, 51–56 (2015).
40. Jenniskens P. Meteor stream activity. *Astron. Astrophys* 287, 990–1013 (1994).
41. Holsapple KA The scaling of impact processes in planetary science. *Annu. Rev. Earth Planet. Sci* 21, 333–373 (1993).
42. Hanner M. & Zolensky M. in *Astromineralogy* (ed. Henning T.) 203–232 (Springer, 2010).
43. Cintala MJ Impact-induced thermal effects in the lunar and mercurian regoliths. *J. Geophys. Res* 97, 947–973 (1992).
44. Lange MA, Lambert P. & Ahrens TJ Shock effects on hydrous minerals and implications for carbonaceous meteorites. *Geochim. Cosmochim. Acta* 48, 1715–1726 (1985).
45. Poston MJ et al. Temperature programmed desorption studies of water interactions with Apollo lunar samples 12001 and 72501. *Icarus* 255, 24–29 (2015).
46. Slyuta EN et al. Application of thermodesorption mass spectrometry for studying proton water formation in the lunar regolith. *Geochem. Int* 55, 27–37 (2017).

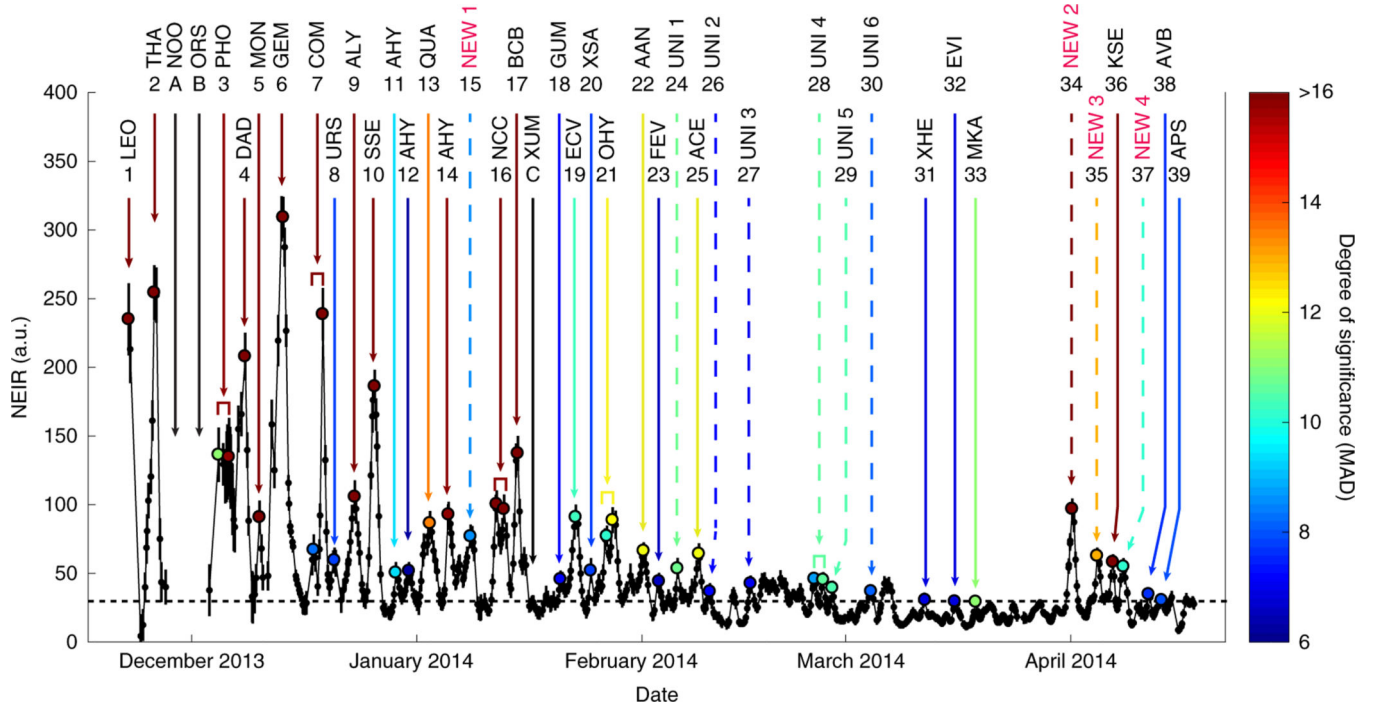


Fig. 1 |. identification of meteoroid streams in NMS-recorded water events.

The NEIR reveals atypical peaks with statistical significance $>6 \times \text{MAD}$. Data points are coloured according to their statistical significance. Solid arrows indicate the point at which each established stream occurred. Streams are identified by their IAU code. Supplementary Table 1 provides their corresponding names. The six dashed arrows labelled as unidentified (UNI) 1–6 do not correspond to any established stream. Streams 15, 34, 35 and 37 (labelled as NEW 1–4) are believed to be new streams. Streams A and B occurred while the NMS was not operational. Established stream C was undetected. The dashed line represents the median NEIR. The error bars (black) reflect the 3σ uncertainty due to counting statistics and data processing. a.u., arbitrary units.

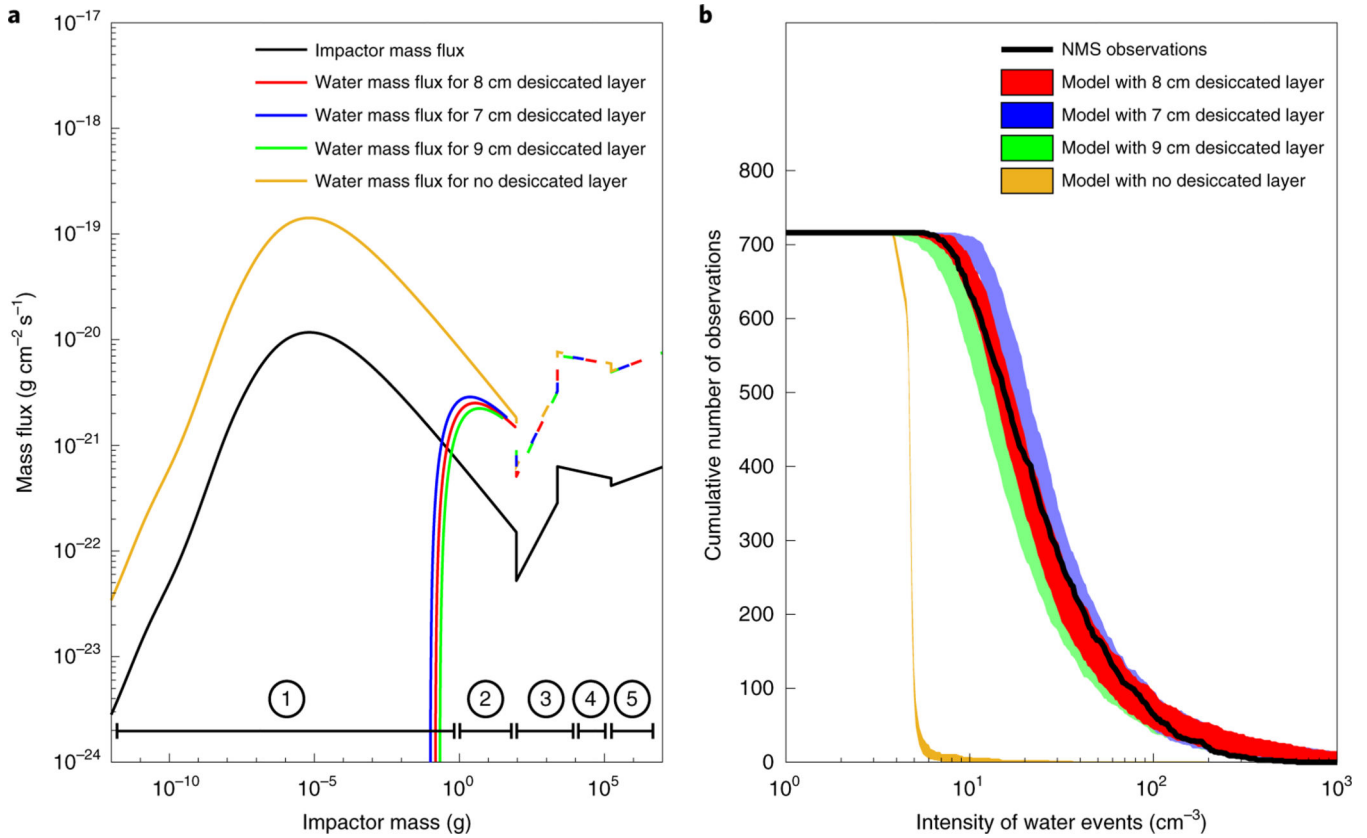


Fig. 2 | Comparison between NMS water event observations and soil hydration models.
a, A mass flux distribution model of impacting meteoroids, constructed by combining the model of Grün et al.³⁴ (range 1) and its extrapolation (range 2), the model of Halliday et al.³⁵ (range 3) and its extrapolation (range 4), and the model of Brown et al.³⁶ (range 5). Water mass fluxes were calculated for lunar surfaces with desiccated top layers of 0, 7, 8 and 9 cm thicknesses. Dashed lines highlight the mass range of large impactors that are insensitive to the presence of a desiccated layer. In the absence of a desiccated layer, the water mass flux is dominated by contributions from meteoroids in the 10⁻⁸–10⁻² g mass range. The inclusion of a dry top layer precludes any water release from meteoroids of <0.15 g. Impactor water mass fluxes were calculated assuming an initial exospheric water vapour temperature $T_e = 5,000$ K. These fluxes will scale down by a factor of 2.3 for $T_e = 500$ K. **b**, Models with desiccated layers replicate the cumulative distribution of the observed water events. An 8.0-cm-thick desiccated layer provides the best fit. The derived hydration $H = 520$ ppm for $T_e = 5,000$ K, and $H = 220$ ppm for $T_e = 500$ K. In the absence of a dry top layer, the distribution of the water events matches that of the duration of the periods of instrument inactivity (Supplementary Fig. 10). For each, the shaded areas depict the range of variation of event distributions for 100 randomly generated mission timelines. Note that results from the model with no desiccated layer in **b** were scaled down in intensity by a factor 100.

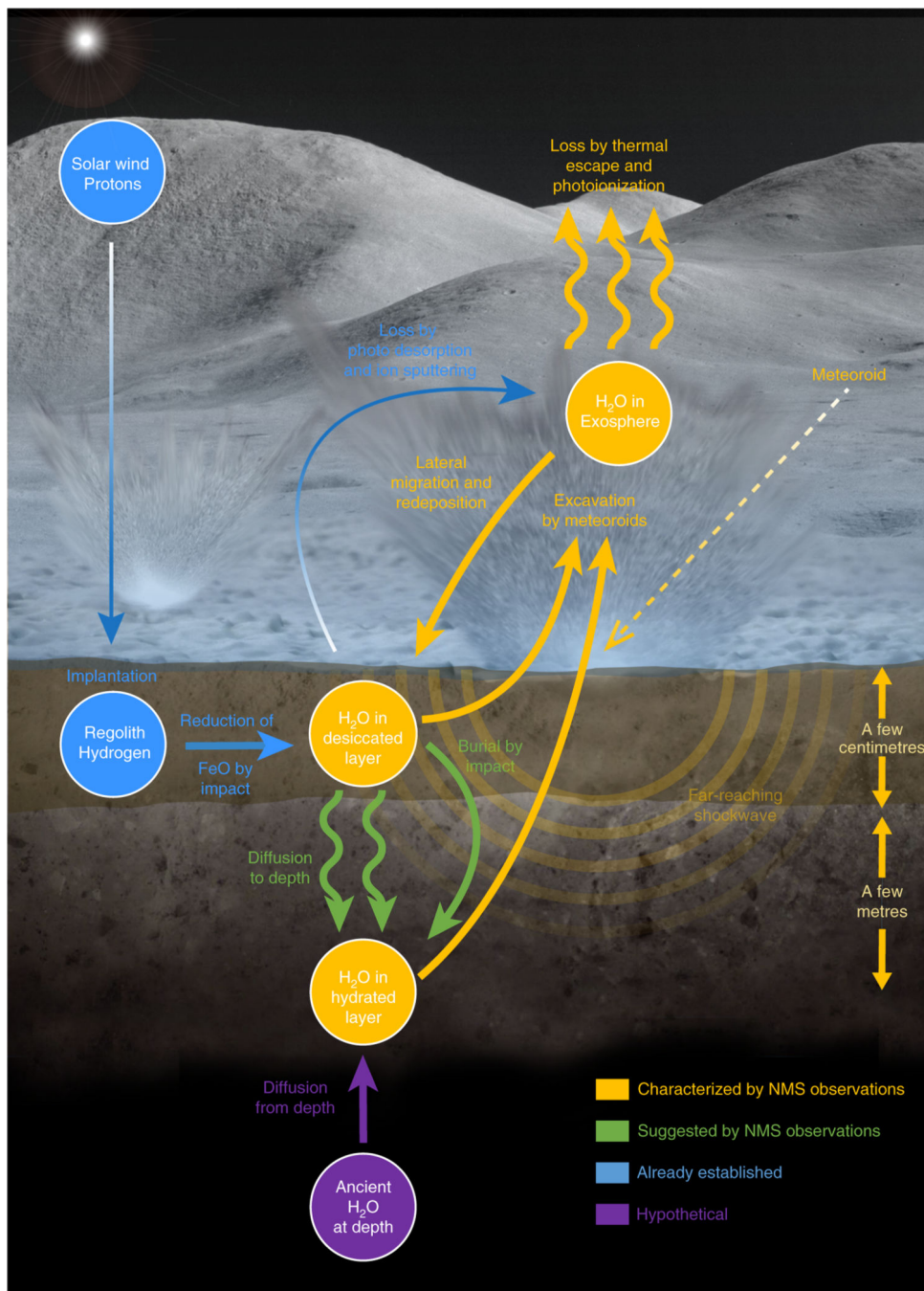


Fig. 3 |. The lunar water cycle as suggested by the NMS observations.
 The cycle relies on the existence of a desiccated strata overlaying hydrated soils. Solar wind-implanted hydrogen is the main exogenous source of water production. Synthesized water diffuses vertically, and can be sequestered in the hydrated layer or lost at the surface. Water from the hydrated soil is extracted by the far-reaching shockwaves generated by large micrometeoroids that strike the surface. The liberated water escapes or is redeposited

elsewhere. To sustain water loss from meteoroid impacts, the hydrated soil layer requires replenishment from a deeper ancient water reservoir.